Nonlinear Dyn (2023) 111:19225–19247
https://doi.org/10.1007/s11071-023-08873-1

ORIGINAL PAPER

Mutual information-assisted feed-forward cascaded stochastic resonance for large parameter

Jian Suo · Haiyan Wang · Xiaohong Shen · Yongsheng Yan · Haitao Dong

Received: 18 April 2023 / Accepted: 29 August 2023 / Published online: 15 September 2023

Abstract Enhancing weak signals submerged in solid background noise is a critical research area in underwater sonar and related applications. Stochastic resonance (SR) has been proven effective in this context, and cascaded stochastic resonance (CSR) offers improved filtering performance. However, CSR faces challenges with low-frequency interference and coupling with the resonance effect of each layer. To address these issues, we propose a novel mutual information-assisted feed-forward cascaded stochastic resonance (MIFF-CSR) method for enhancing weak signals in large-parameter conditions. MIFF-CSR utilizes mutual information between the high-pass filtered SR output and the original noisy signal to mitigate low-frequency interference and exploit the beneficial properties of SR. Furthermore, MIFF-CSR decouples CSR's dependence on each layer, progressively improving the signal-to-noise ratio by feeding forward the original signal to each cascaded SR layer. Simulations demonstrate the effectiveness of MIFF-CSR in solving low-frequency interference problems and its robust band-pass filtering characteristics for weak signal enhancement. The relationship between MIFF-CSR output and the number of cascaded layers confirms its signal enhancement capabilities. Additionally, MIFF-CSR exhibits high tolerance to the selection of cascaded layers and high-pass filter cut-off frequency. MIFF-CSR significantly enhances filtering performance, frequency response characteristics, and anti-noise capabilities compared to CSR. Application verification experiments were conducted to validate the effectiveness and practicality of the proposed method, which showed significant improvements in application performance.

Keywords Cascaded stochastic resonance · Input feed-forward · Cross spectrum · Weak underwater signal · Low signal-to-noise ratio (SNR)

J. Suo · H. Wang · X. Shen · Y. Yan · H. Dong
School of Marine Science and Technology, Northwestern Polytechnical University, Youyi West Road, Xi'an 710072, Shaanxi, China
e-mail: jiansuo@mail.nwpu.edu.cn

H. Wang
e-mail: hywang@sust.edu.cn

X. Shen
e-mail: xhshen@nwpu.edu.cn

Y. Yan
e-mail: ysyan@nwpu.edu.cn

J. Suo · X. Shen · Y. Yan
Key Laboratory of Ocean Acoustics and Sensing (Northwestern Polytechnical University), Ministry of Industry and Information Technology, Youyi West Road, Xi'an 710072, Shaanxi, China

H. Wang
School of Electronic Information and Artificial Intelligence, Shaanxi University of Science and Technology, Xi'an 710021, Shaanxi, China

H. Dong (✉)
School of Electronic Engineering, Xidian University, Xi'an 710071, Shaanxi, China
e-mail: hai3water@126.com

1 Introduction

Enhancing weak signals is a fundamental area of research with broad applications in various fields [1–3]. Notably, it is critical in applications such as sonar where the enhancement of weak signals, including underwater ship radiated noise, is vital [4]. In recent years, stochastic resonance (SR) [5] has emerged as a novel nonlinear signal processing method that departs from conventional filtering-based approaches to signal processing. It adopts the concept of "noise being beneficial" and exploits noise to enhance signals, demonstrating significant potential, particularly in processing signals with low signal-to-noise ratios (SNR) and in-band noise [6]. This characteristic has attracted numerous scholars to pursue research in this area [7].

SR is a nonlinear phenomenon that arises from the synergistic interaction of signals, noise, and nonlinear systems, leading to an enhanced output [8]. The concept was initially proposed by Benzi et al. [9]. As of now, SR has transitioned from being a theoretical concept to a practical area of research with diverse engineering applications [5,7,10,11]. While SR offers promising advantages, its application is constrained by the requirement of small parameter values. Specifically, the signal frequency and amplitude must be significantly lower than one, which is unrealistic for most engineering signals. For instance, the frequency of underwater ship radiated noise usually falls within the range of 70–1000 Hz [12]. To address the engineering limitations of SR, researchers have proposed several large-parameter SR methods based on system parameter tuning [13]. These methods include re-scaling frequency SR [14], step-changed SR [15], frequency-shifted, and re-scaling SR [16], which have significantly enhanced the feasibility of single SR for engineering applications.

With the deepening research on weak signal processing methods using SR, researchers have discovered that complex SR systems, composed of multiple SR systems that cooperate, exhibit superior performance compared to a single SR system. Typical representatives of complex SR systems include cascaded stochastic resonance (CSR) [17–19], coupled SR [20–23], globally coupled parallel SR [24], feedback SR [25,26], SR array [27,28], and SR in neuronal networks [29,30]. Additionally, SR networks composed of cascade and array connections are essential for developing complex SR with better performance. CSR involves serially connecting multiple SR systems to achieve multi-stage filtering and gradually improve SNR [18,31]. In contrast to individual SR methods, the progressive operational framework [32,33] of CSR has shown substantial efficacy in enhancing waveform smoothness. This strategic approach has garnered significant research attention and broad application across diverse domains [34–36]. Moreover, this progressive operational strategy has found significant application within deep learning. For instance, it has been effectively employed in designing the wavelet multi-resolution super-resolution network, which captures auxiliary information from diverse subspaces, uncovers multi-resolution and multi-domain features, and employs a progressive approach to reconstruct super-resolution images [37]. Similarly, the deep Laplacian pyramid super-resolution network progressively reconstructs the sub-band residuals of super-resolution images at multiple pyramid levels [38]. Therefore, the comprehensive study of CSR, especially focused on performance improvement, is of great theoretical and practical significance.

Despite the superior performance of the CSR system in weak signal processing, the issues related to CSR under large parameter conditions have not received adequate attention and resolution. Most focus has been on addressing large parameter issues concerning individual SR. Under large parameter conditions, the CSR system consistently transfers high-frequency energy to low-frequency, thereby amplifying the inherent Lorentzian characteristics of SR [39,40]. This amplification results in low-frequency interference that overwhelms the target signal, making effective extraction challenging. This phenomenon becomes even more pronounced under large parameter conditions, significantly compromising the CSR's ability to effectively extract weak signals amidst strong background noise. In addition, due to the sustained amplification of SR's Lorentzian characteristics by the CSR system under large parameter conditions, a significant amount of strong low-frequency interference existing in the signal transmits to the subsequent layer. These interferences are particularly likely to dominate the response of the subsequent layer's SR, resulting in a sustained deterioration of the subsequent SR's resonance effect. As a result, its effectiveness in restoring the target signal is compromised. Therefore, the information forwarded layer by layer by CSR exhibits low efficiency and value. Furthermore, the response of CSR is significantly influenced by the resonance of each layer within the CSR system, particularly at the

initial layer [19]. Specifically, inadequate resonance at any layer of the CSR system, especially the first layer, can cause subsequent layers to transfer high-frequency energy to low-frequency only, ultimately resulting in the failure to recover the target information and exacerbating the low-frequency interference on the target information. These problems are highly coupled and severely limit the application of CSR in engineering.

In order to address the issue of limited engineering applications of CSR under large parameter conditions, this paper proposes a novel mutual information-assisted feed-forward cascaded stochastic resonance (MIFF-CSR) method. It is a framework of cascaded SR with mutual information assistance and original information feed-forward. In this framework, the output signals of each SR layer undergo high-pass filtering, and the distinct distributions between the filtered SR output signals and the original signals are ingeniously utilized to extract mutual information. The signals containing mutual information and the original noisy signals with complete target information are then jointly input into the subsequent SR layer, thereby progressively enhancing the signal. As the information contained in the output signals of each SR layer cannot be guaranteed to be only the target information, extracting the mutual information from both the output signals and the original signals markedly mitigates interference input to the subsequent layer. Simultaneously, the feed-forward of original noisy signals guarantees the inclusion of complete target information in each layer. After conducting a comparative analysis with SR, CSR, and CSR with high-pass filter methods, MIFF-CSR demonstrates superior performance. The unique advantages of MIFF-CSR can be summarized as follows: (1) effectively suppresses low-frequency interference and decouples the dependence on SR effectiveness in each layer, enhancing signal processing stability; (2) high tolerance in selecting cascade layers and high-pass filter cutoff frequency, providing a broader frequency response range and improved characteristics suitable for practical applications like limited sampling rates; (3) performs better in large parameter conditions, exhibiting superior band-pass filtering and anti-noise performance. It can efficiently extract weak spectral features from heavy background noise, producing cleaner output signals.

The remaining sections of the paper are organized as follows. Section 2 provides an overview of traditional CSR and large-parameter SR and analyzes their Lorentzian characteristics and first-layers dependence. Section 3 presents the proposed mutual information-assisted feed-forward cascaded stochastic resonance (MIFF-CSR) method for large parameters and explains its principles. Section 4 focuses on the simulation analysis and comparative verification of MIFF-CSR, traditional CSR, and CSR assisted by high-pass filtering. Section 5 validates the proposed method through experiments and provides discussion. Section 6 concludes the paper.

2 Large parameter CSR

2.1 Large parameter SR with bistable model

The classical bistable stochastic resonance (CBSR) is a phenomenon that exploits the energy of noise to amplify weak signals amidst background noise, achieved through the synergistic interplay of the nonlinear system, signal, and noise. CBSR can be viewed as a nonlinear filtering process with a nonlinear response, which is described by an overdamped Langevin equation [39],

$$\frac{\mathrm{d}x}{\mathrm{d}t} = -\frac{\mathrm{d}U(x)}{\mathrm{d}x} + s(t) + \Gamma(t) \tag{1}$$

where x denotes the output of the system, while $s(t) = A\cos(2\pi f_0 t + \phi)$ refers to an externally periodic weak signal with parameters A, f_0, and ϕ indicating the signal's amplitude, driving frequency, and initial phase, respectively. The term $\Gamma(t)$ represents additive Gaussian white noise (AWGN) with zero means, where $\langle \Gamma(t)\Gamma(t+\tau)\rangle = 2D\sigma(t)$ and D represents the noise intensity and τ is the time interval. The potential function $U(x)$ is characterized by a double well shape,

$$U(x) = -\frac{a}{2}x^2 + \frac{b}{4}x^4 \tag{2}$$

where the parameters a and b in CBSR can be tuned to optimize the system's output signal by matching the signal and noise. The function has one possible inflection point at $x_0 = 0$ and two local minima located at $\pm\, x_{\mathrm{m}}$.

Assume that the input noisy signal contains a weak periodic signal $s(t) = A_0\cos(w_0 t)$, and the output signal of the CBSR system is,

$$\langle x(t)\rangle = \overline{x}(D)\cos(w_0 t - \overline{\varphi}) \tag{3}$$

where $\bar{x}(D)$ and $\bar{\varphi}(D)$ can be expressed as

$$\begin{cases} \bar{x}(D) = \dfrac{A_0 x_m^2}{D} \cdot \dfrac{2r_{\mathrm{K}}}{\sqrt{(2r_{\mathrm{K}})^2 + w_0^2}} \\ \bar{\varphi}(D) = \arctan\left(\dfrac{w_0}{2r_{\mathrm{K}}}\right) \end{cases} \tag{4}$$

where r_{K} is the Kramers rate [39], $x_m = \sqrt{a/b}$, D is the noise intensity. The Kramers rate of CBSR can be written as

$$r_{\mathrm{K}} = \frac{1}{\sqrt{2}\pi} \exp\left(-\frac{\Delta U}{D}\right), \tag{5}$$

where $\Delta U = a^2/4b$. Under the small parameter condition, the power spectral density of the output from the SR system can be obtained by taking the Fourier transform of the autocorrelation function [39],

$$\begin{aligned} \mathrm{S}(\omega) &= \mathrm{S}_n(\omega) + \mathrm{S}_s(\omega) \\ &= \left[1 - \frac{1}{2}\left(\frac{A_0 x_m}{D}\right)^2 \frac{4r_{\mathrm{K}}^2}{4r_{\mathrm{K}}^2 + \Omega^2}\right] \frac{4r_{\mathrm{K}} x_m^2}{4r_{\mathrm{K}}^2 + \omega^2} \\ &\quad + \frac{\pi}{2}\left(\frac{A_0 x_m}{D}\right)^2 \frac{4r_{\mathrm{K}}^2 x_m^2}{4r_{\mathrm{K}}^2 + \Omega^2} \\ &\quad [\sigma(\omega - \Omega) + \sigma(\omega + \Omega)] \end{aligned} \tag{6}$$

where the function $S_n(\omega)$ is obtained by multiplying a Lorentzian distribution derived in the absence of an input signal ($A_0 = 0$) with a scaling factor dependent on the forcing amplitude A_0, constrained to values less than unity. In contrast, the function $S_s(\omega)$ represents the synchronous periodic response induced by external periodic excitation. Notably, the total output power, which encompasses both the signal and noise components of the two-state model under investigation, is a constant value of $2\pi x_m^2$ and is not influenced by the amplitude or frequency of the input signal (A_0 and ω, respectively).

The output SNR defined as Eq.(7) is adopted as the measurement index of SR,

$$\mathrm{SNR} = 10\log_{10}\left(\frac{A_0}{\sum_{i=1}^{N/2} A_i - A_0}\right) \tag{7}$$

where A_0 represents the amplitude of the target signal frequency f_0 in the output power spectrum, the item $\sum_{i=1}^{N/2} A_i - A_0$ denotes the amplitude sum of noise in the output power spectrum, and N is the length of the noisy signal.

Since actual signals do not comply with the conditions of SR in the small parameter limit, the RFSR method [14] applies a linear compression on high frequencies based on an appropriate frequency scale factor R to convert high frequencies into low frequencies that satisfy the conditions of SR in the small parameter limit. Specifically, assuming that a noisy signal $s_n(t)$ contains a periodic signal with frequency f_0 and that the signal is sampled at a rate of f_{s}, the time interval of the discrete data and the step size for solving the fourth-order Runge–Kutta (RK4) equation [41] are both $1/f_{\mathrm{s}}$. By introducing the frequency scaling factor R ($R > 1$), the RK4 solver's step becomes redefined as $h' = R/f_{\mathrm{s}}$. In this way, the time interval of the signal can be readjusted ($f_{\mathrm{s}}' = f_{\mathrm{s}}/R$) while also achieving compression of the periodic signal's frequency by a factor of R, i.e., $f' = f_0/R$. Consequently, the original signal $s_n(t)$ is transformed into a new signal $s_n'(t)$ with frequency f' and sampling rate f_{s}', which becomes a low-frequency signal that satisfies the small parameter condition of SR. With an appropriate scaling factor R that determines the values of f_{s}' and f_0', this type of signal can trigger the emergence of SR in bistable systems. The scaling factor R selection can be referenced from the literature [14].

2.2 Low-frequency interference and each-layer dependence in CSR

SR can effectively enhance weak signals by utilizing noise under small parameter conditions. However, CBSR will suffer from severe low-frequency interference under large parameter conditions. Figure 1 displays a set of noisy signals with a signal frequency of $f_0 = 200$ Hz and a sampling rate of $f_{\mathrm{s}} = 50$ kHz. It is evident that the temporal waveform is disrupted by random noise, but the frequency domain reveals distinct spectral lines (as indicated by the red circle). The signal processed using the GA optimized SR approach [42], as shown in Fig. 2a, exhibits distinct Lorentzian characteristics. Within this characterization, the transference of high-frequency energy to low frequencies is evident, resulting in the emergence of significant low-frequency interference.

CSR can be understood as a multi-stage filtering process, where the signal is sequentially passed through a series of cascaded SR systems, as illustrated in Fig. 4a. The CSR output for the first, second, third, and fifth layers is presented in Fig. 2a–d for the given noisy signal in Fig. 1, revealing both the time-domain and frequency-

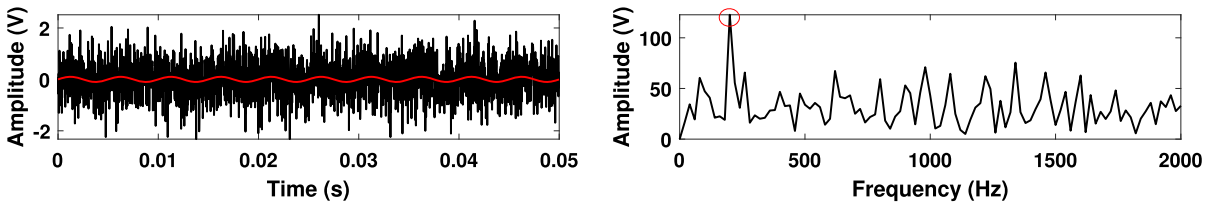

Fig. 1 The simulated noisy signal and corresponding frequency spectrum, the red wave denotes pure signal

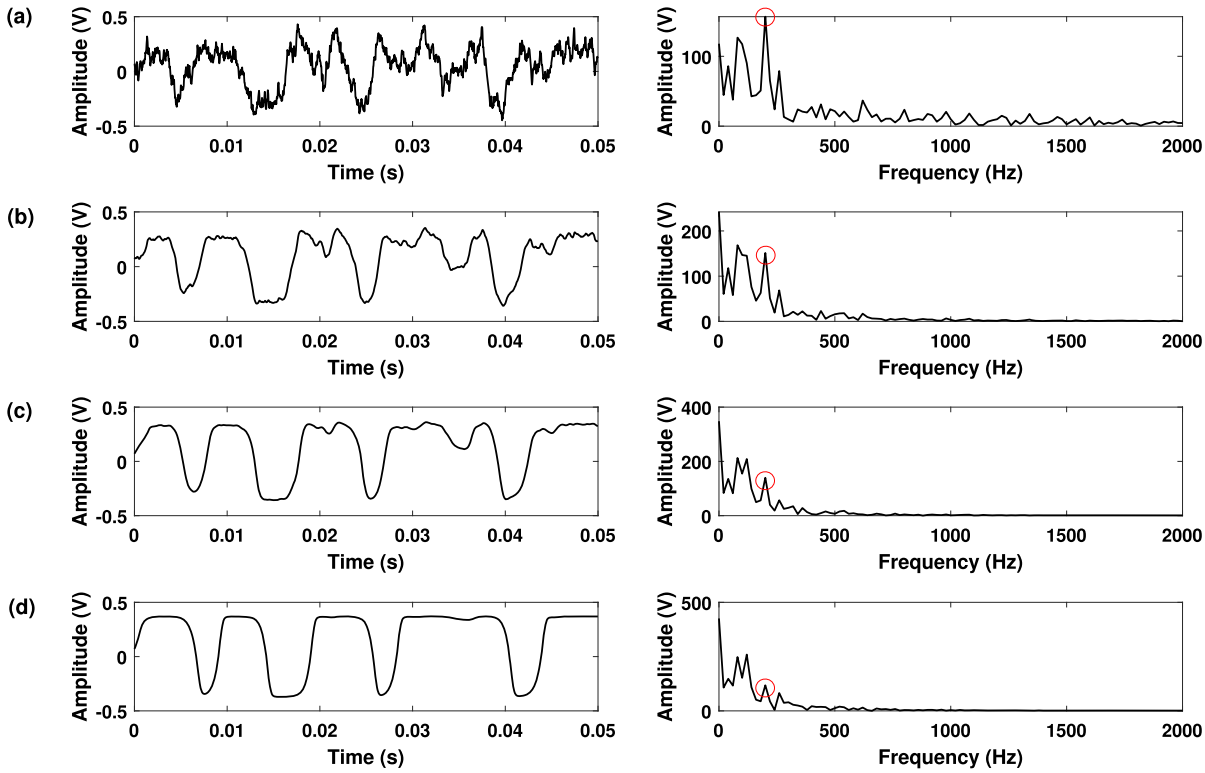

Fig. 2 The low-frequency interference of CSR: **a** the output of first layer, **b** the output of second layer, **c** the output of third layer, **d** the output of fifth layer (scaling factor $R = 2000$)

domain characteristics. Figure. 2a serves as both the output of the classical single SR and the first-layer output of CSR, allowing for a comparison between SR and CSR. Notably, it can be seen from Fig. 2a–d that the Lorentzian properties persist within the CSR system under conditions of large parameters and are more prominently displayed compared to a single SR system. Moreover, as the number of cascaded layers increases, low-frequency interference becomes increasingly pronounced. From another perspective, the information transfer between CSR layers is suboptimal.

In the presence of low-frequency interference, high-pass filtering is often considered a straightforward solution. To evaluate the effectiveness of a high-pass filter-assisted CSR system, we conducted simulations based on its schematic diagram as shown in Fig. 4b. The output results are presented in Fig. 3, where Fig. 3a shows the output of the first layer SR (shared with a single SR system), and Fig. 3b displays the result after applying a high-pass filter with a cutoff frequency of 100 Hz. It is worth noting that a 120 Hz spectral peak is generated in the signal after passing through the high-pass filter, slightly higher than the cutoff frequency. This spectral feature is distinctly magnified by the second-layer SR, as illustrated in Fig. 3c. However, when the signal from Fig. 3c undergoes further processing with an additional

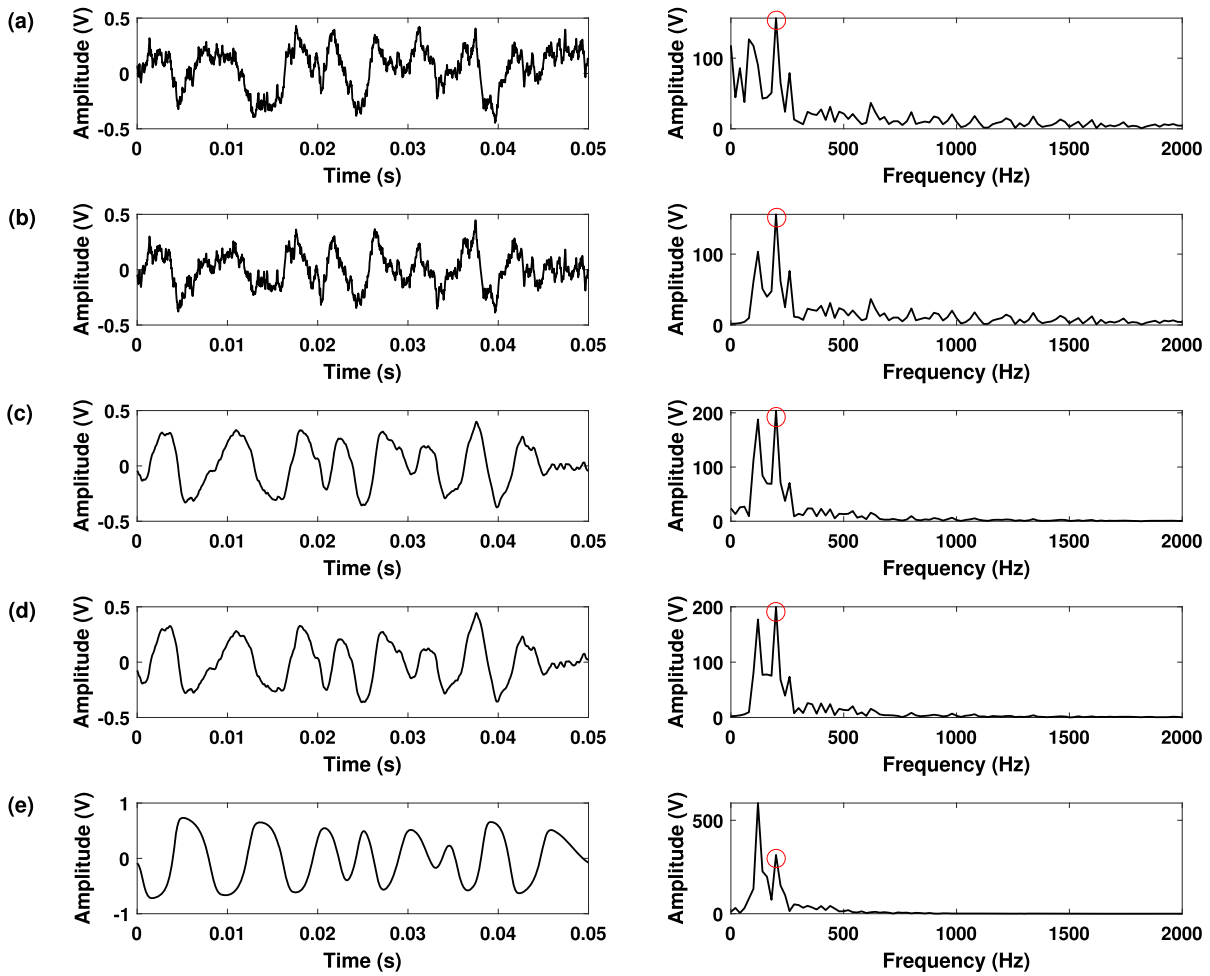

Fig. 3 The low-frequency interference of CSR with high-pass filter assisted: **a** the output of first layer, **b** first-layer SR output after high-pass filter processing, **c** the output of second layer, **d** second-layer SR output after high-pass filtering, **e** the output of fifth layer

SR layer, the resulting output, illustrated in Fig. 3d, does not enhance the discrimination between the 120 Hz spectral peak and the target frequency (as indicated by the red circle). After five consecutive layers of processing, as depicted in Fig. 3e, the amplitude of the 120 Hz spectral peak intensifies significantly, surpassing that of the target peak. This intensification poses the potential risk of hindering the extraction of the target signal. Consequently, the high-pass filter-assisted CSR system proves inadequate in effectively mitigating the interference introduced by the high-pass filter, resulting in the submersion of the target spectrum and subsequent failure of detection.

In summary, regardless of whether it is a CSR or a high-pass filter-assisted CSR system, severe low-frequency interference exists under large parameter conditions, and this interference becomes increasingly severe as the number of cascade layers increases. Furthermore, as demonstrated by the schematic diagram and the results in Figs. 2 and 4a, the CSR heavily relies on the output of each layer, especially the first layer. When the desired resonance effect is absent in the first layer, subsequent layers predominantly transfer high-frequency energy to low frequencies, failing to restore the signal waveform or rectify the issues within the first layer. In addition, the transfer of information between CSR layers is suboptimal due to the transmission not

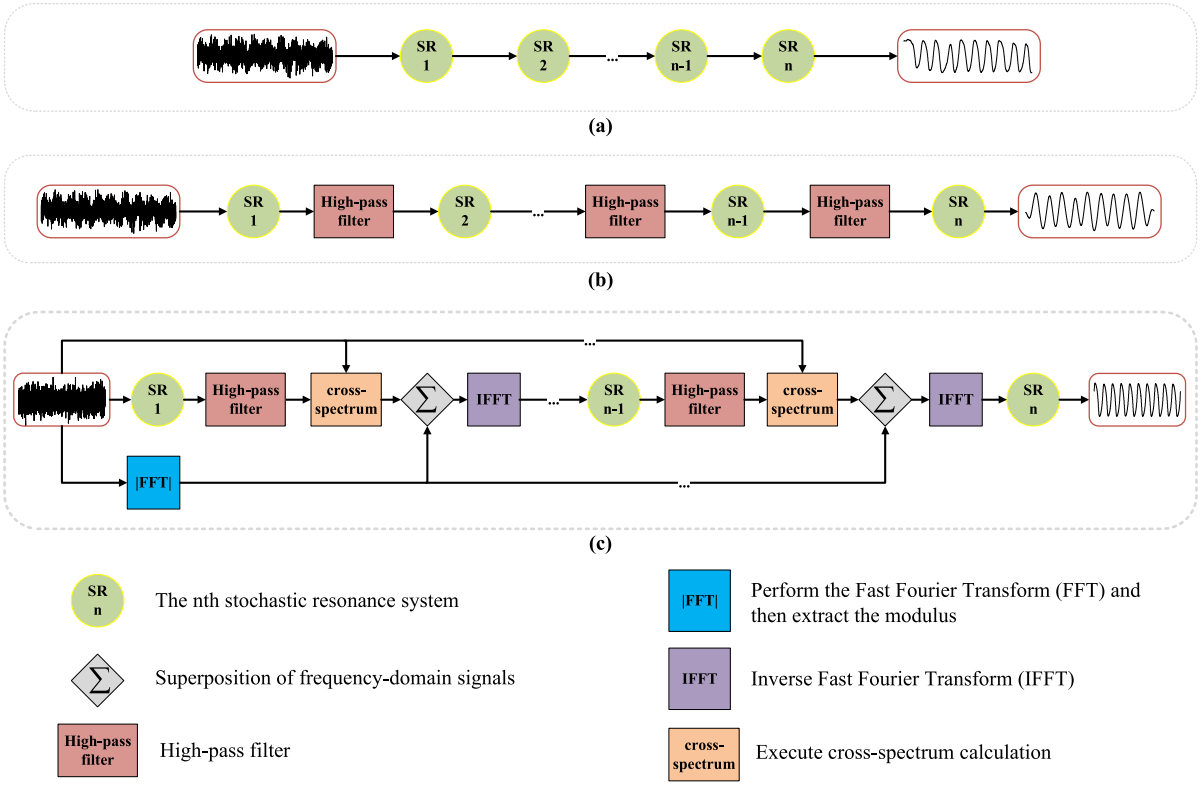

Fig. 4 The framework: **a** CSR, **b** CSR with high-pass filter, **c** MIFF-CSR

only of the desired signal but also of a considerable amount of low-frequency interference.

3 MIFF-CSR method

As analyzed in the previous section, conventional CSR systems are markedly influenced by the Lorentzian property, resulting in strong low-frequency interference under large parameter conditions. Despite attempts at mitigation through the integration of high-pass filtering, effectively eliminating such interference remains a challenge. In addition, the significant reliance on the resonance effect of the first layer and the suboptimal forward information transmission scheme represent notable limitations in CSR systems. This section proposes a novel MIFF-CSR method to overcome these limitations.

3.1 Framework of MIFF-CSR

MIFF-CSR represents a modified version of the conventional CSR system that seeks to overcome its inherent drawbacks. Specifically, MIFF-CSR achieves complete target information at each layer by forwarding the original noisy signal to every layer while applying high-pass filtering to remove low-frequency interference caused by SR under large parameter conditions. Moreover, MIFF-CSR performs cross-spectrum analysis between the original noisy signal and the SR output at each layer to extract mutual information, which is then used as input for the subsequent layer. Lastly, MIFF-CSR aligns signal phases in the frequency domain, enabling constructive summation. The mathematical model of MIFF-CSR is presented as Eq.(8), and the corresponding principle schematic is shown in Fig. 4c,

$$\begin{cases} \mathrm{d}x_1(t)/\mathrm{d}t = -\partial U\,(x_1)\,/\partial x_1 + sn(t) \\ \mathrm{d}x_i(t)/\mathrm{d}t = -\partial U\,(x_i)\,/\partial x_i + y_{i-1}(t) \\ y_{i-1}(t) = \mathcal{F}^{-1}\left\{|SN(\omega)| + \mathrm{Re}[\mathrm{SN}(\omega)\cdot P_{i-1}(\omega)^*]\right\} \\ P_{i-1}(\omega) = H(\omega)X_{i-1}(\omega) \quad i = 2, 3, \ldots, L. \end{cases} \tag{8}$$

In Eq. (8), $U(x)$ denotes the potential function of the SR system as shown in Eq. (2). The original received noisy signal that requires processing is denoted as $sn(t) = s(t) + n(t)$, where $s(t)$ is the desired target signal and $n(t)$ is the noise component. The transformation of $s(t)$ through the Fast Fourier Transform (FFT) manifests as $\mathrm{SN}(\omega)$. The frequency domain representation of the output signal at the $(i-1)$th layer of the SR system, following the application of a high-pass filter, is denoted as $P_{i-1}(\omega)$. The real part of a complex variable is denoted by $\mathrm{Re}(\cdot)$ and $\mathrm{Re}[\mathrm{SN}(\omega)\cdot P_{i-1}(\omega)^*]$ represents the cross-spectrum operation performed on these two signals and then acquire the real part. The output signal of the ith layer SR system in the time domain is represented as $x_i(t)$, while its FFT is denoted as $X_{i-1}(\omega)$. $H(\omega)$ represents the frequency response function of the high-pass filter. The input signal of the ith layer SR system ($i > 1$) is represented as $y_{i-1}(t)$. The inverse fast Fourier transform (IFFT) is represented by $\mathcal{F}^{-1}$, while the complex modulo operation is represented by $|\cdot|$, and the conjugate operation is denoted by *.

As detailed in Sect. 2, the outcome of processing a noisy signal using large-parameter SR contains partial or complete target information, and low- and high-frequency interference. The interference mainly arises from the constraints inherent to the signal enhancement capacity of an individual SR system, while the low-frequency interference stems from the prominent Lorentzian characteristics of large-parameter SR. In order to overcome this issue, a high-pass filter is employed to mitigate severe low-frequency interference that can disrupt cascaded systems and be gradually amplified layer by layer, potentially submerging the target signal, as illustrated in Fig. 2. Therefore, filtering out these low-frequency interferences is essential to effectively minimize their adverse impact from the preceding layer's output on the subsequent layer.

However, the use of a high-pass filter introduces new line spectrum interference that can disturb the subsequent cascaded SR systems, as illustrated in Fig. 3. The transmitted signals to the subsequent layer may also contain interference other than the desired target information. This interference may arise from the imperfect performance in the previous SR system or the low-frequency interference resulting from the large parameter SR Lorentzian characteristic. The proposed method attains a twofold objective by employing a cross-spectrum operation to extract mutual information from the unprocessed original signal and the SR output signal after high-pass filtering. Firstly, it effectively suppresses the interference generated by the high-pass filter on the subsequent SR systems. Secondly, it facilitates the transmission of a more refined signal, enriched with target information, to the subsequent processing layer. Consequently, this method effectively mitigates the impact of low-frequency interference stemming from the suboptimal output of the preceding layer on the subsequent layers. The cross-spectrum operation can achieve this effect because the noise distribution between the original signal to be processed and the high-pass filtered SR output signal has significant changes. In theory, only the target signal is present in the mutual part, while the newly introduced low-frequency interference generated by the high-pass filter is absent in the original noisy signal. Therefore, it can be effectively suppressed by extracting common information through cross-spectrum calculation.

On the other hand, although the combination of high-pass filtering and cross-spectrum calculation cleverly minimizes the transmission of other interferences to the next layer, it may also lead to incomplete transmission of target information to subsequent cascaded SR systems. This may impede the extraction of complete target information. Moreover, the performance and stability of CSR are also limited by the dependence on the effectiveness of the first-layer SR. Thus, feeding the original noisy signal forward to each SR layer can enable each layer to possess comprehensive target information, consequently alleviating CSR's dependence on the first layer and facilitating a gradual improvement in the SNR. Furthermore, as the number of cascaded layers in CSR increases, the high-frequency components in the signal, which are then input to the next layer of SR, are continuously shifted to the low frequency, causing the noise-enhancement capability of the system to weaken. Feeding the original signal forward can provide high-frequency noise energy to subsequent cascaded systems.

To fully exploit the benefits of feeding the original signal forward, a frequency-domain method is

employed in our proposed approach to superimpose the cross-spectrum result with the original noisy signal. More specifically, we begin by subjecting the original noisy signal to FFT, followed by the computation of its modulus. Subsequently, we extract the real part of the cross-spectrum result. These steps ensure phase alignment of the two signals before the addition, thereby inducing a constructive effect.

3.2 Signal enhancement demonstration of MIFF-CSR

To better demonstrate the processing procedure of the MIFF-CSR method, this subsection employs a set of simulations for illustration. The simulated signal has a center frequency of $f_0 = 200$ Hz and a sampling rate of $f_s = 50$ kHz. The additive Gaussian white noise has a variance of 1, resulting in an SNR of -26.5094 dB. The original noisy signal is shown in Fig. 5a, where the random noise overwhelms the temporal waveform. The frequency-domain plot displays the spectral line corresponding to the signal frequency f_0, indicated by the red circle. This spectral line remains identifiable despite being disrupted by noise. After the first-layer SR processing, the output is shown in Fig. 5b. The spectral plot clearly shows the Lorentzian characteristics of the large parameter SR, where high-frequency energy is transferred to a low-frequency area, leading to the interference of the target signal frequency f_0 by low-frequency noise. It can also not distinguish the target signal from the temporal waveform due to the interference of low-frequency noise. After performing high-pass filtering on the output signal from the first-layer SR and conducting a cross-spectrum analysis between the filtered SR output signal and the input noisy signal, the cross-spectrum results are added to the input signal. The resulting input signal for the second-layer SR system is illustrated in Fig. 5c, demonstrating suppressed low-frequency interference compared to the SR output shown in Fig. 5b. Thus, the MIFF-CSR method effectively mitigates the impact of low-frequency interference from the suboptimal output of the preceding layer on the subsequent layer.

As the cascaded layers increase, the processing outcomes of the MIFF-CSR method are illustrated in Fig. 5d–g. The spectral plots depict a continuous reduction in high-frequency interference and a significant attenuation of low-frequency interference. The MIFF-CSR second and third-layer output results, shown in Fig. 5d and e, exhibit a further restoration of the temporal waveforms along with substantial interference reduction. A clear sinusoidal waveform can be observed, and the spectral peak at f_0 is further enhanced, with low-frequency and high-frequency interference far lower than the target signal. The fourth and fifth layer outputs are shown in Fig. 5f and g, respectively, where the interference, especially low-frequency interference, is further reduced, resulting in a more shaped temporal waveform, sharper spectral line at f_0, and an improved SNR from the original -26.5094 to 2.2147 dB at the fifth layer output. The entire processing procedure demonstrates that the proposed MIFF-CSR method can gradually improve the SNR, restore the signal waveform, and effectively solve the severe low-frequency interference problem in the large parameter SR, showcasing pronounced band-pass filtering characteristics.

The SNR of both the input and output signals at each layer of MIFF-CSR, shown, respectively, as solid and dashed lines with black circular markers in Fig. 6, demonstrates a rising trend with increasing cascaded layers. Moreover, the output SNR curve surpasses the input SNR curve, indicating the progressive improvement in SNR achieved by MIFF-CSR. To further validate the efficacy of reducing the impact of low-frequency interference in the suboptimal output of the previous layer on the subsequent layer, we introduce a novel indicator termed $\mathrm{SNR_L}$. It is defined as the logarithm of the ratio between the energy at the target frequency, denoted by f_0, and the total energy of all low-frequency interference below f_0 (as expressed in Eq. (9)). This indicator offers a degree of insight into the severity of low-frequency interference.

$$\mathrm{SNR_L} = 10\log_{10}\left(\frac{A_0}{\sum_{i=1}^{N_0} A_i}\right) \tag{9}$$

where A_0 represents the amplitude of the target signal frequency f_0 in the output power spectrum. $\sum_{i=1}^{N_0} A_i$ denotes the sum of low-frequency noise amplitudes below f_0 in the output power spectrum. Here, $N_0 = N_t f_0/f_s$ represents the length of low-frequency interference in the frequency domain, with N_t being the length of the noisy signal in the time domain. The $\mathrm{SNR_L}$ of each layer's output signal in MIFF-CSR is depicted as solid lines with red rectangular markers in Fig. 6. Additionally, the $\mathrm{SNR_L}$ of the corresponding output signal, undergoing high-pass filtering and subsequent cross-spectrum analysis with the original sig-

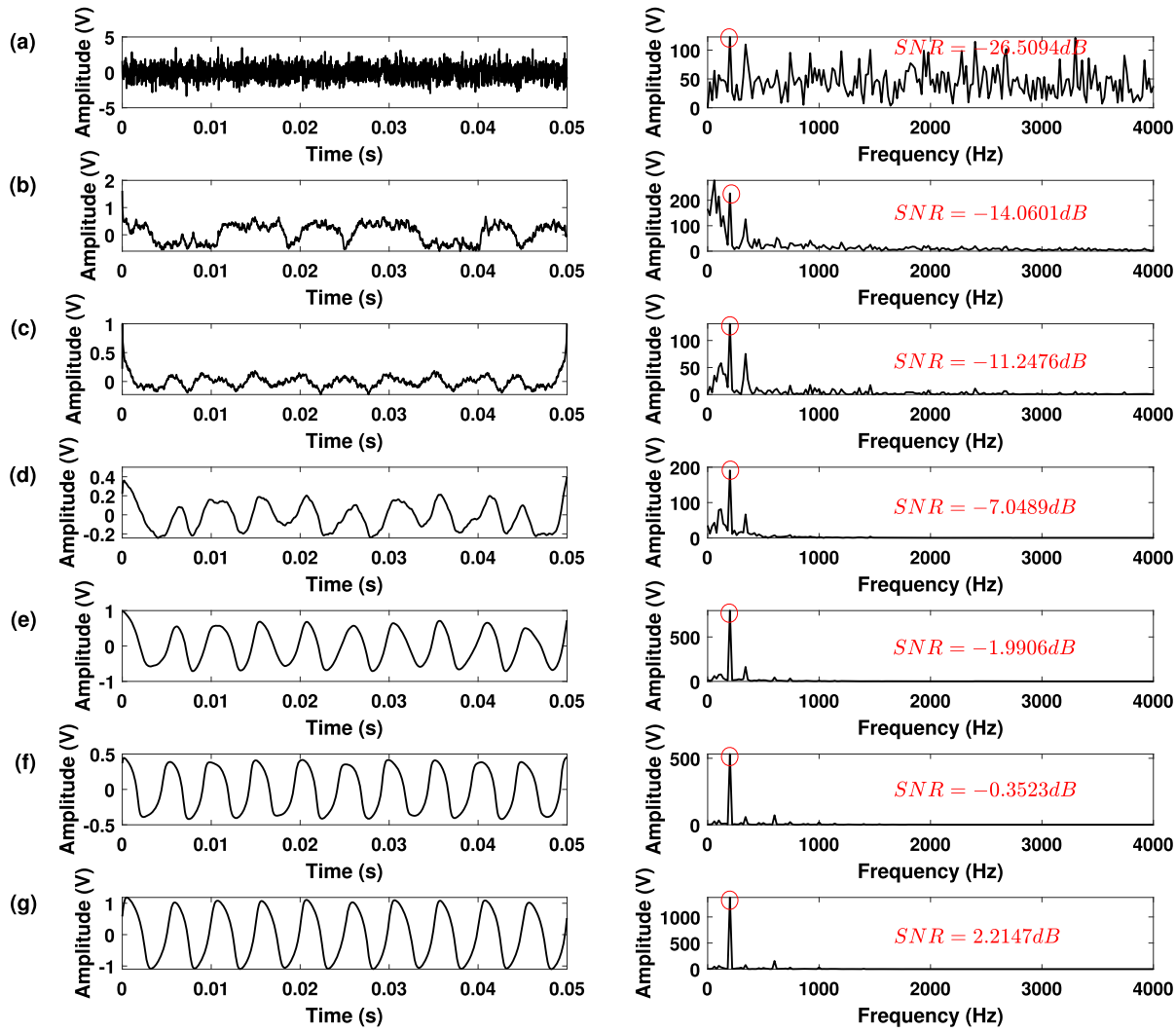

Fig. 5 The output results of each layer of the MIFF-CSR system during the processing: **a** Time-domain waveform and frequency spectrum of the noisy signal to be processed, **b** Time-domain waveform and frequency spectrum of the first layer output, **c** Time-domain waveform and frequency spectrum obtained by high-pass filtering the first-layer output, cross-spectrum with the original signal, and subsequently superimposing with original signal, **d**-**g** Time-domain waveform and frequency spectrum of the output from the second to the fifth layer

nal, is represented by dashed lines with red rectangular markers in Fig. 6. It is evident from the graph that the former curve consistently remains positioned below the latter, demonstrating that the processed output, serving as the input for the subsequent layer, experiences reduced low-frequency interference compared to the previous SR output. This substantiates the effectiveness of the proposed method in mitigating the impact of low-frequency interference in the suboptimal output of the previous layer on the subsequent layer.

3.3 Implementation flow of the proposed MIFF-CSR method

Building upon the preceding analysis, this subsection introduces a signal-processing workflow that employs the MIFF-CSR method. The workflow is depicted in Fig. 7, and its implementation is delineated through the subsequent steps:

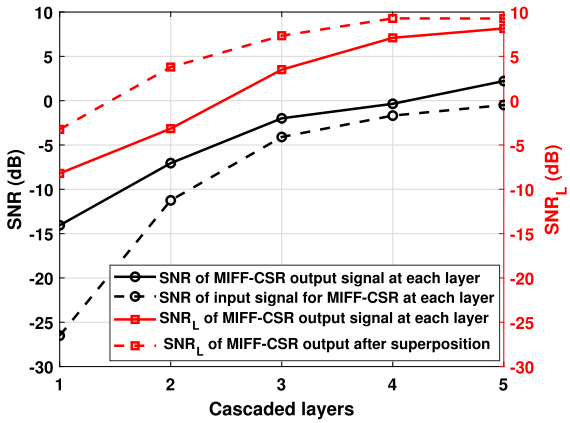

Fig. 6 The SNR of MIFF-CSR input and output signals varies with the number of cascaded layers (represented by black lines with circles). The red solid line within red squares corresponds to SNR_L of the output signal at each layer, focusing on low-frequency interference. Additionally, the red dashed line within red squares depicts the variation of SNR_L for the signal obtained by high-pass filtering, cross-correlation, and superimposition of the output signal with the original signal

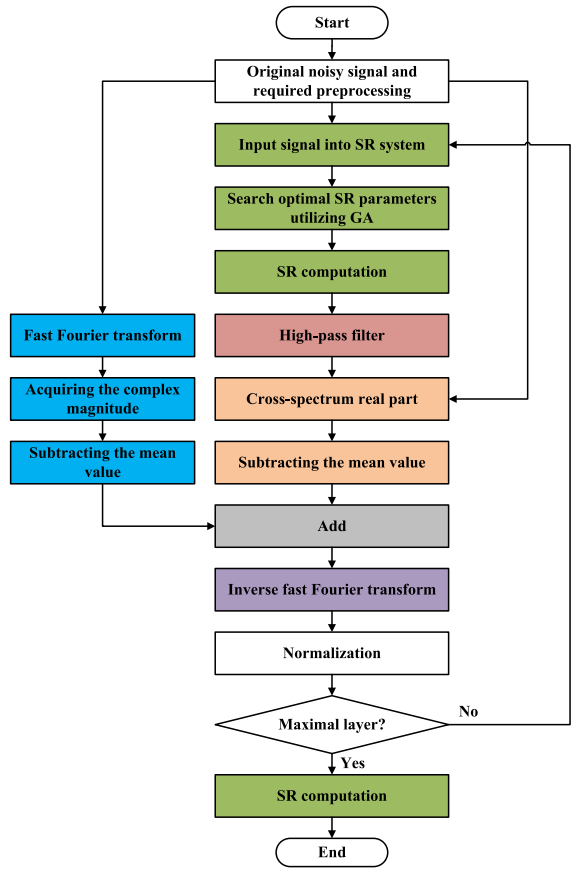

Fig. 7 The implementation flow of MIFF-CSR method

(1) Signal pre-processing: Various signal processing techniques may be employed to pre-process the received signal, such as DC component removal, signal normalization, and envelope extraction, depending on the specific requirements of the application.
(2) Parameter initialization: In all simulations and experiments, SR parameters a and b are GA-searched within the range of [0.01, 5], with a population size of 50 and a terminal generation size of 10. The maximum number of cascaded layers for subsequent signal-processing layers is also established.
(3) SR computation: The signal is processed using SR, and the commonly used GA algorithm is applied to optimize the SR system parameters. The optimal waveform, corresponding to the maximum SNR, is then outputted.
(4) High-pass filtering: The SR output signal obtained in Step (3) is subjected to high-pass filtering.
(5) Cross-spectrum and its real part calculation: The real part of the cross-spectrum between the original received signal and the output signal obtained in Step (4) is calculated.
(6) Signal addition and normalization: The DC component is removed from the original received signal, and a fast Fourier transform is performed, followed by modulus calculation. The results of this step are added to the real part of the cross-spectrum calculated in Step (5). An inverse Fourier transform is then carried out, and the resulting signal is normalized.
(7) Cascaded layer processing: Steps (3) to (6) are repeated until the maximum number of cascaded layers is reached.
(8) Last layer processing: The output signal obtained from Step (6) is fed into the SR system, where the GA algorithm is applied to optimize the system parameters. The resulting optimized waveform, corresponding to the maximum SNR, is then generated as the final output of the signal processing workflow.

4 Simulation analysis and evaluation

To validate and evaluate the performance of the proposed MIFF-CSR method, this section comprehensively assesses various aspects of MIFF-CSR, including the number of cascaded layers, the impact of high-pass filter cutoff frequency on MIFF-CSR, frequency response, filtering performance, and anti-noise performance. Except for the simulation of the number of cascaded layers in Sect. 4.1, the maximum number of cascaded layers in other simulations is set to 5. In addition, for the CSR and high-pass filter-assisted CSR, the ultimate output is determined based on the layer with the highest SNR among the five layers, while for MIFF-CSR, the output of the fifth layer is considered. Additionally, the ensuing simulations are conducted using Matlab R2022b on a platform equipped with the following parameters: Intel i7-8700 CPU @ 3.20 GHz Quad Core processor, 8-GB memory, 64-bit-win10 operating system.

4.1 Analysis of MIFF-CSR enhancement with varying cascaded layers

This subsection primarily conducts simulation analysis on the variation of the output SNR with the number of cascaded layers for the proposed method. The aim is to validate the processing flow and the role of cascading, as well as to determine the generally required number of cascaded layers to support future applications. The simulation parameters are set as follows: signal amplitude $A = 0.1$, signal frequency $f_0 = 200$ Hz, sampling frequency $f_s = 50$ kHz, scaling factor $R = 2000$, and noise variance $\sigma^2 = 1$ and $\sigma^2 = 2$, respectively. The data length is $N = 2500$ points, and the cutoff frequency of the high-pass filter is set to $fp = 100$ Hz. The average results of 100 independent simulations are presented in Fig. 8. From Fig. 8a and c, it can be observed that the conventional CSR achieves the optimal output SNR at the second layer, and the high-pass filter-assisted CSR achieves the optimal output SNR at the third layer, under different noise variance. However, the proposed MIFF-CSR method already surpasses the optimal output SNR of both CSR and high-pass filtered CSR at the second layer, demonstrating a significant advantage in achieving faster SNR improvement. This observation is highly consistent with the original intention of designing the MIFF-CSR method based on the concept of mutual information feed-forward. Furthermore, a comparison of the final output SNRs reveals that the proposed MIFF-CSR method significantly outperforms the other two methods, demonstrating its superior performance in enhancing weak signals.

Figure 8b and d depicts the absolute value of the cross-correlation coefficient between the output signal at each layer and the original pure sinusoidal signal, with noise variance $\sigma^2 = 1$ and $\sigma^2 = 2$, respectively. This parameter quantifies the similarity between the two signals, with a higher value signifying enhanced system performance. From the figure, it is evident that the proposed MIFF-CSR method consistently outperforms the other two methods in terms of cross-correlation coefficient, indicating a higher similarity between the final optimal output signal and the original pure signal. Moreover, the proposed MIFF-CSR method demonstrates a more rapid rate of improvement in similarity compared to the other two methods. These findings further substantiate the superior performance of the proposed method in waveform recovery.

Additionally, upon comparing Figs. 8a to d, it can be observed that the proposed method requires a relatively stable number of cascaded layers, which is around 5–6. Additional layers do not lead to significant performance improvements but do not cause adverse effects as in traditional CSR. Therefore, the proposed method does not impose stringent requirements on the number of cascaded layers in general. Nonetheless, in scenarios where achieving resonance poses challenges, especially when the ratio of sampling frequency to signal frequency is relatively small, a higher number of cascaded layers becomes imperative to achieve satisfactory SNR levels. Figure 9 presents a simulation of the output SNR variation with cascaded layers under the following parameters: the signal frequency f_0 = 315 Hz, sampling frequency f_s = 12 kHz, scaling factor $R = 1000$, signal amplitude A=0.1, noise variance $\delta^2 = 2$, the signal length $N = 4800$ points, and high-pass filter cutoff frequency $fp = 250$ Hz. Notably, the simulation reveals an optimal number of cascaded layers at 22 in MIFF-CSR, and further cascading does not lead to adverse effects. The comprehensive analysis shows that fewer cascaded layers suffice under favorable conditions facilitating SR, whereas scenarios with limited sampling rates hindering SR necessitate more cascaded layers. Furthermore, a system with too few cascaded layers may underutilize its perfor-

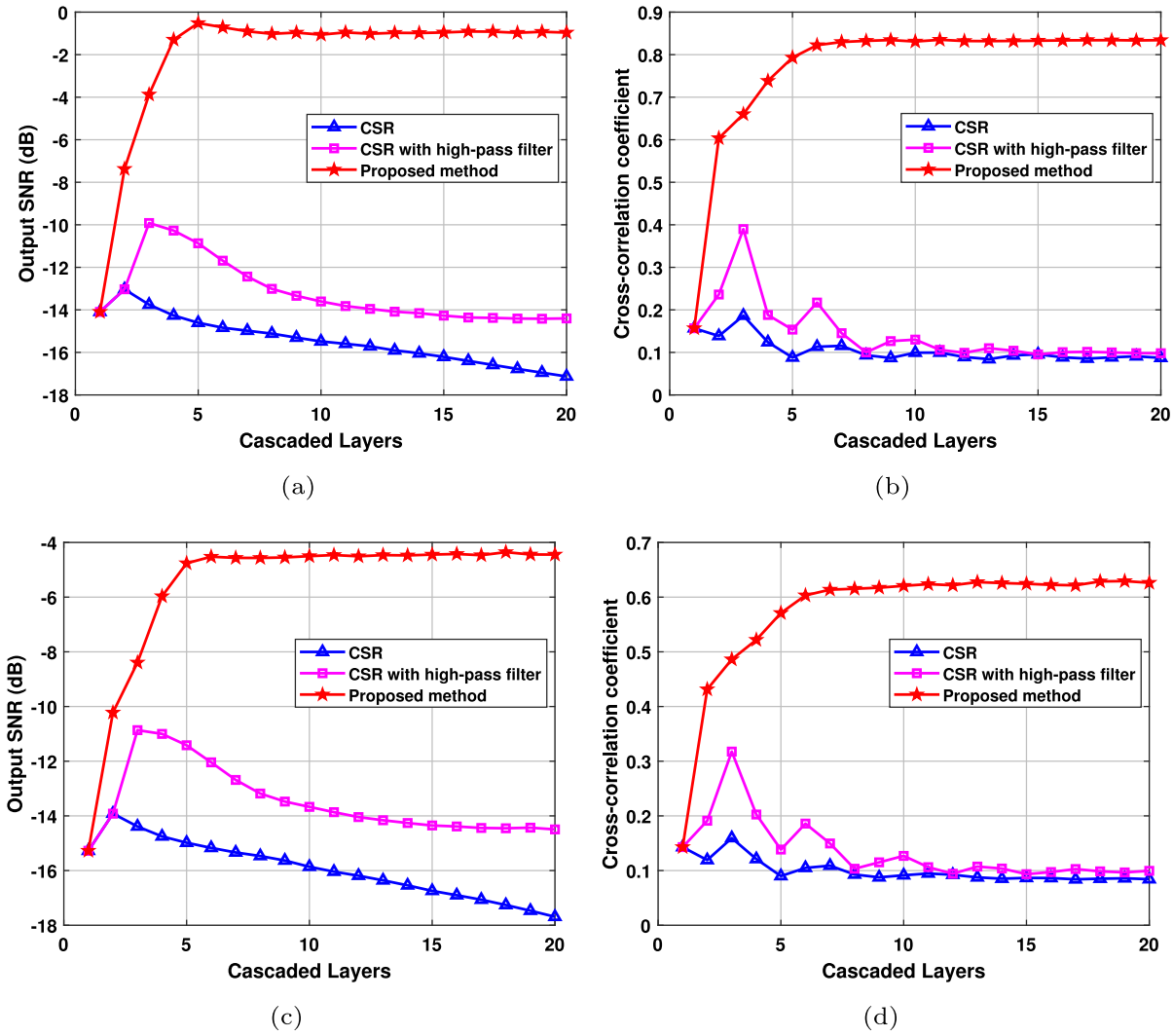

Fig. 8 Variation of output SNR and similarity with respect to cascade layer number: **a** $\sigma^2 = 1$, output SNR with layers, **b** $\sigma^2 = 1$, the correlation coefficient with pure signal, **c** $\sigma^2 = 2$, output SNR with layers, **d** $\sigma^2 = 2$, the correlation coefficient with pure signal

mance potential, resulting in insufficient enhancement of noisy signals to higher SNR. Conversely, a system with excessive cascaded layers unleashes its performance effectively without incurring the adverse effects observed in CSR. However, excessive cascading does not translate to boundless performance improvement and may lead to inefficient utilization of computational resources. Thus, the practical selection of cascaded layers demands a judicious balance between signal characteristics and computational capacities. Moreover, the simulation presented in Fig. 9 reaffirms another advantage of MIFF-CSR over SR and CSR: it exhibits superior signal enhancement capabilities at limited sampling rates, albeit requiring a higher number of cascaded layers.

4.2 The cutoff frequency of high-pass filter analysis

In the proposed MIFF-CSR approach, the high-pass filter plays a crucial role, and its impact on the signal enhancement performance of MIFF-CSR is an important issue to investigate. To this end, we conducted 1000 independent simulations with the high-pass filter cutoff frequency ranging from 40 Hz to 180 Hz in 20 Hz increments. The remaining simulation parame-

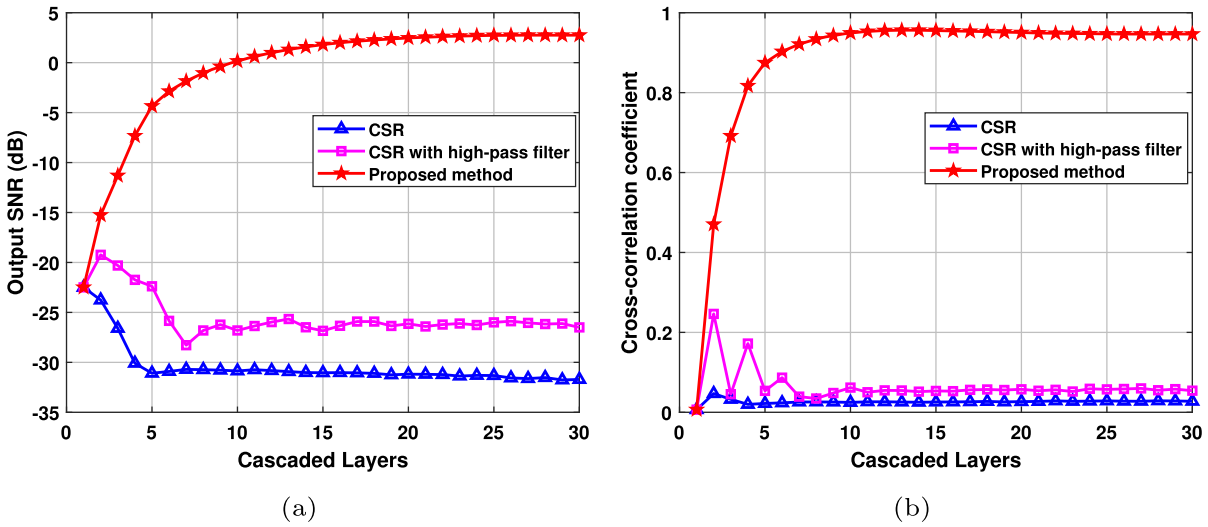

Fig. 9 Variation of output SNR and similarity with respect to cascade layer number under limited sampling rate: **a** $\sigma^2 = 1$, output SNR with layers, **b** $\sigma^2 = 1$, the correlation coefficient with pure signal

ters remained consistent with those detailed in Fig. 8, except for the variance of Gaussian white noise, set to $\sigma^2 = 1$. The average simulation results are shown in Fig. 10, showcasing the propensity of the proposed MIFF-CSR method to maintain a nearly stable output SNR across varying high-pass filter cutoff frequencies. This implies that any reasonable selection of the filter cutoff frequency can lead to the optimal output. Therefore, the proposed method has low dependence on the choice of high-pass filter cutoff frequency. As a general guideline, it is advisable to choose the cutoff frequency of the high-pass filter within the range of $0.5\,f_0$ to $0.8\,f_0$. In contrast, the CSR with high-pass filter method shows a modest enhancement in output SNR as the cutoff frequency of the high-pass filter increases, compared to the CSR. Additionally, the comparison between the curve of the CSR with high-pass filter-assisted and that of the high-pass filter at low cutoff frequencies indicates that the high-pass filter-assisted CSR has a higher output SNR, demonstrating the necessity of introducing the high-pass filter in the SR system. At higher cutoff frequencies, the output SNR of the high-pass filter-assisted CSR is consistent with the high-pass filter, suggesting that the improvement in the output SNR is predominantly attributable to the high-pass filter under such conditions. Overall, the proposed MIFF-CSR method exhibits superior performance compared to the CSR with a high-pass filter assisted at any cutoff frequency, validating the high tolerance of the proposed method to the selection of the cutoff frequency of the high-pass filter as well as its superior performance.

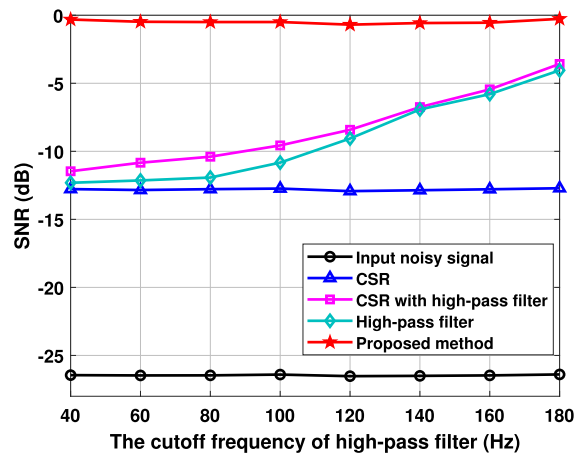

Fig. 10 The variations of output SNR with high-pass filter cutoff frequency

4.3 Frequency response analysis

Due to the wide frequency range of the target signal in practical applications, frequency response analysis is necessary and critical. Further simulation analysis of the frequency response is conducted with the following parameters: $A = 0.3, \sigma^2 = 1, f_s = 50$ kHz,

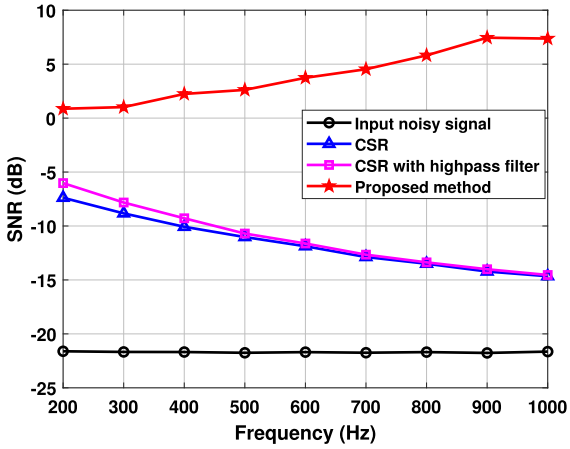

Fig. 11 Frequency response analysis

$N = 2500$, and $R = 5000$. The signal frequency f_0 ranges from 200 Hz to 1000 Hz in 100 Hz increments. The cutoff frequency of the high-pass filter is set as $fp = 100$ Hz. The average results of 100 independent simulations are shown in Fig. 11. From the figure, it is evident that both the CSR and CSR with high-pass filter assistance methods exhibit diminishing output SNR as the input signal frequency increases. In contrast, our proposed MIFF-CSR method shows a continuously increasing output SNR as the input signal frequency increases, which indicates the excellent frequency response characteristic of our proposed MIFF-CSR method. This means the traditional CSR method is unable to solve the Lorentzian characteristic present in SR, which becomes increasingly pronounced as the signal frequency increases, even with high-pass filter assistance. Furthermore, due to the fixed cutoff frequency of the high-pass filter, the performance curves of both CSR and high-pass filter-assisted CSR gradually overlap as the signal frequency increases, indicating a diminishing improvement in SNR due to the high-pass filter. This also implies that the improved performance of the high-pass filter-assisted CSR over the traditional CSR in Fig. 10 is mainly attributed to the high-pass filter rather than the synergy between the high-pass filter and CSR. This further illustrates the limited effectiveness of the high-pass filter-assisted CSR in processing high-frequency signals. In contrast, our proposed MIFF-CSR method, leveraging a well-coordinated cross-spectrum operation and high-pass filtering, effectively addresses this challenge, resulting in an output response that remains unaffected as the signal frequency increases. The continuous increase in output with rising frequency can be attributed to the large scaling factor R, further highlighting the potential of our proposed method for stable operation at high frequencies and under limited sampling rate conditions, thus demonstrating its strong potential for practical engineering applications.

4.4 Filtering performance analysis and evaluation

In order to evaluate the filtering performance of the proposed MIFF-CSR method, a set of noisy signals with a noise variance of 4 and signal amplitude of 0.1 were tested. The signal frequency was set to $f_0 = 200$ Hz, the sampling frequency was set to $f_s = 50$ kHz, the signal length was 2500 points, and the scale factor was R=2000. The original noisy signal, as shown in Fig. 12a, has an SNR of −28.5844 dB, and its time-domain waveform was chaotic and disordered, with the periodic signal completely submerged by noise. In the frequency domain, the target frequency was also submerged by numerous interference, making it impossible to identify the target frequency information accurately.

To restore the periodic signal waveform and extract the target frequency information, the noisy signal was processed using SR, CSR, CSR with high-pass filtering, and the proposed MIFF-CSR. The time-domain waveform and frequency spectrum data of a single SR output are shown in Fig. 12b. The periodic signal is not distinctly discernible in the time-domain waveform, and in the frequency spectrum, the high-frequency energy is transferred to the low-frequency region due to the Lorentzian characteristic of the SR output, which reduces the influence of high-frequency interference on the target frequency information. However, it also leads to more serious low-frequency interference, which completely submerges the target frequency information.

CSR exclusively transfers the high-frequency energy to the low-frequency region again, further reducing the high-frequency interference and smoothing the output waveform. However, it simultaneously intensifies the low-frequency interference, as shown in Fig. 12c. Although the SNR is improved after CSR processing, the ability to identify and detect the target frequency information diminishes notably.

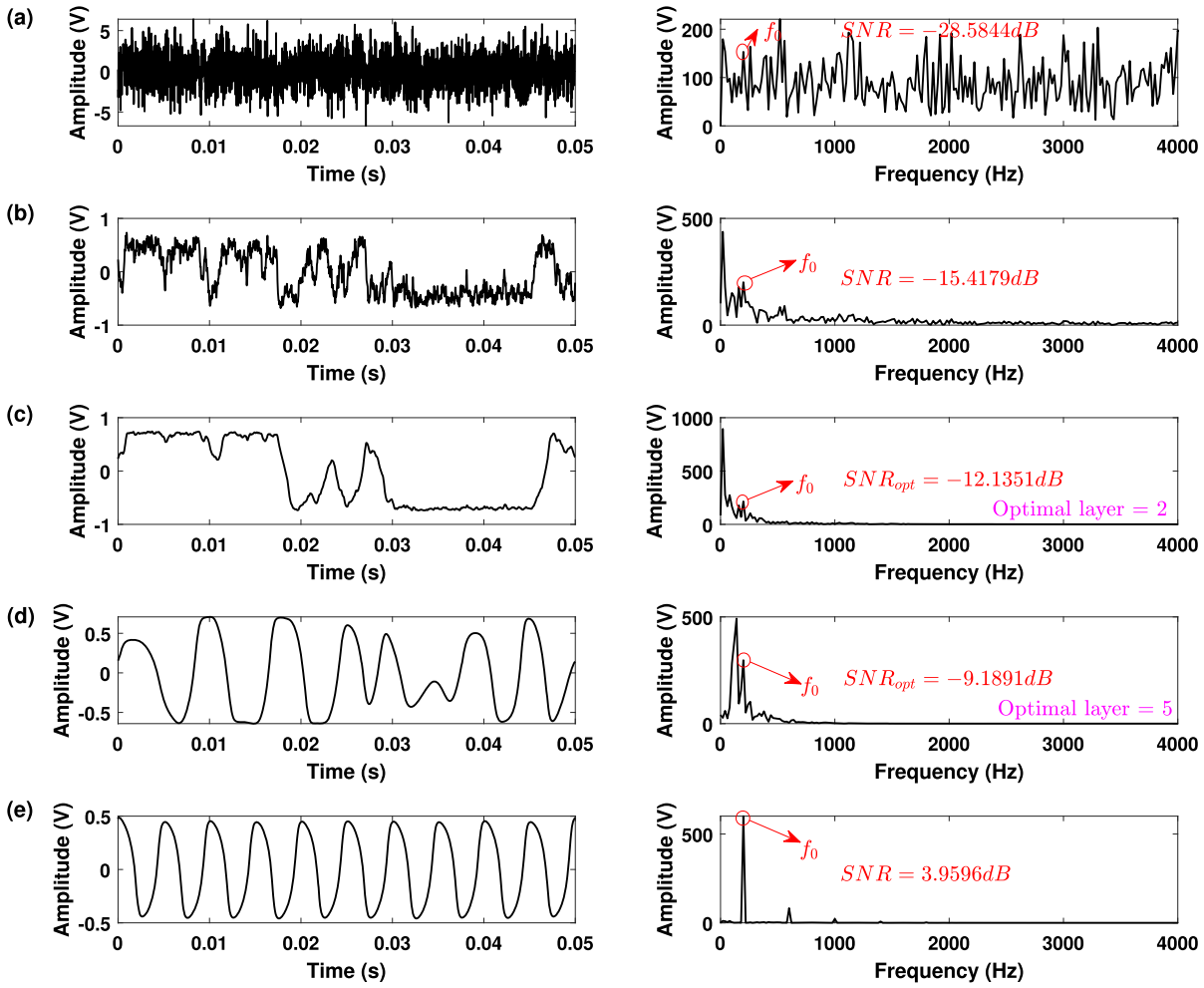

Fig. 12 Comparison of filtering performance among SR, CSR, CSR with high-pass filter and proposed MIFF-CSR

In order to mitigate low-frequency interference in CSR, a high-pass filter with a cutoff frequency of $fp = 100$ Hz is introduced. Figure 12d shows the output of CSR with high-pass filter assistance, which exhibits a periodic waveform caused by low-frequency interference in the frequency domain. The high-pass filter eliminates low-frequency interference caused by the Lorentzian characteristic in CSR. However, a strong interference slightly higher than the cutoff frequency emerges, making it challenging to identify the target frequency information accurately.

The outcomes of the proposed MIFF-CSR processing are shown in Fig. 12e. It can be observed from the figure that the time-domain waveform has been effectively restored after being processed by the MIFF-CSR system. Both excessive low-frequency and high-frequency interferences have been effectively filtered out, and the target frequency is distinctly discernible from the spectral line at the designated frequency. The amplitude of the target frequency spectrum considerably surpasses than that of other methods. Although weak interferences exist at odd multiples of the target frequency, they do not affect the extraction of the target frequency and can be easily filtered out. From the perspective of SNR improvement, the proposed MIFF-CSR method demonstrates a higher output SNR, surpassing SR by 19.38 dB, CSR by 16.09 dB, and high-pass filter-assisted CSR by 13.15 dB. This outcome further solidifies the excellent filtering characteristics of MIFF-CSR. The comparative filtering performance results demonstrate that the proposed MIFF-CSR method can effectively extract large-parameter

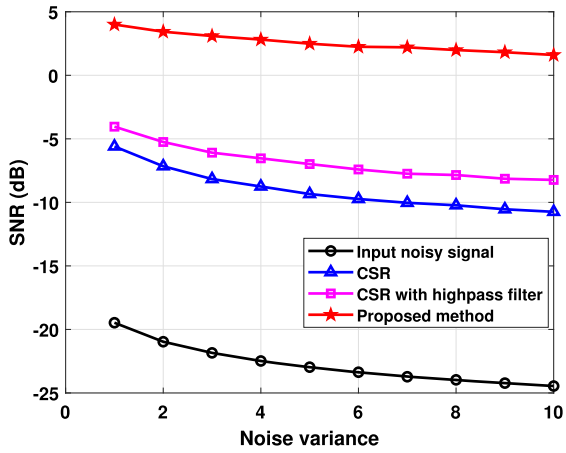

(a)

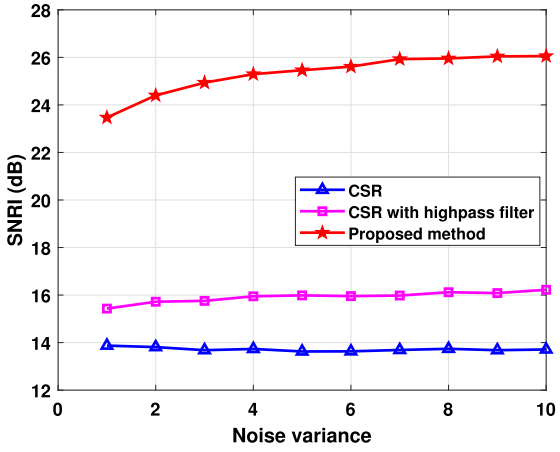

(b)

Fig. 13 Comparison of anti-noise performance: **a** Output SNR varies with noise variance, **b** SNR improvement varies with noise variance

signals from strong background noise and significantly improve the filtering performance.

4.5 Anti-noise performance analysis

In practical scenarios, the intensity of background noise constantly fluctuates due to environmental changes. Therefore, signal processing methods with robust anti-noise capabilities assume paramount importance. The anti-noise performance of CSR, CSR assisted by high-pass filtering, and the proposed MIFF-CSR method is compared in Fig. 13a. Here, the signal amplitude A is kept constant at 0.5, the variance of Gaussian white noise is varied from 1 to 10 with a step of 1, the signal frequency f_0 is 200 Hz, the sampling rate f_s is 50 kHz, the scaling factor R is 2000, and the cut-off frequency of the high-pass filter fp is 100 Hz. It can be clearly seen from Fig. 13a that the proposed MIFF-CSR method exhibits better performance, with its output SNR curve being higher than those of CSR and CSR assisted by high-pass filtering. Moreover, the output SNR curves of all methods slowly decrease as the noise variance increases. However, the proposed MIFF-CSR method decreases more slowly than the other two methods, as seen more clearly from the SNR improvement curve in Fig. 13b. This indicates that the proposed MIFF-CSR method has better anti-noise performance, which is advantageous for practical engineering applications and extracting weak signals from strong background noise.

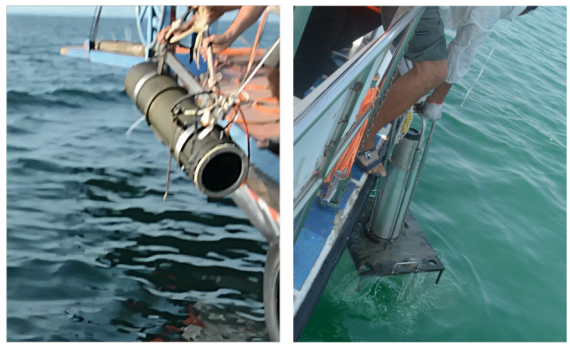

(a) (b)

Fig. 14 The equipment used in the experiment: **a** UW350, **b** Receiver

5 Application verification and discussion

5.1 Application verification

In order to validate the effectiveness and adaptability of the proposed method, a set of experiments was conducted at Danjiangkou Reservoir using UW350 acoustic sources, as shown in Fig. 14a. The UW350 emits a single-frequency spectral signal with a frequency of $f_0 = 315$ Hz. The hydrophone, as shown in Fig. 14b, was positioned on the bottom of the water as the receiver, which received the signal at a sampling rate of $f_s = 12$ kHz from a distance of 6 km. Additionally, the hydrophone has a low-pass filtering circuit with a cutoff frequency of 2 kHz. The original noisy sig-

nal received by the hydrophone is depicted in Fig. 15a, clearly indicating the presence of the target signal in the frequency domain with a relatively high SNR. To accurately assess the performance of the proposed method, we selected a segment of environmental noise that is temporally proximate to the target signal and originates from the same environment. Subsequently, the selected environmental noise is amplified by a factor of five, as shown in Fig. 15b and superimposed onto the hydrophone's received noisy signal, thereby constructing a signal to be processed with a comparatively lower SNR. After removing the DC component, the resulting superimposed signal to be processed is shown in Fig. 16a. It is evident from the figure that the target signal is entirely masked by noise in the time-domain waveform. In contrast, the interference around the target line spectrum could potentially impede accurate identification in the frequency domain.

The signal shown in Fig. 16a undergoes processing using the proposed MIFF-CSR method alongside SR, CSR, and CSR with high-pass filter methods for comparative analysis. The MIFF-CSR method employed a 30-layer cascaded structure, with the output from the 25th layer serving as the final result. Both the CSR and high-pass filter-assisted CSR methods utilized a 5-layer cascaded structure, selecting the output with the highest SNR from these five layers as the final result. The cutoff frequency of the high-pass filter in both the MIFF-CSR and high-pass filter-assisted CSR methods is set to $f\mathrm{p} = 250$ Hz. A rescaling ratio of $R = 1000$ is uniformly applied across all the methods. The parameters for the GA are set as follows: an initial population size of 50, a searching range of [0.01, 5] for the SR parameters a and b, and a maximum of 10 generations. The resulting time-domain waveform and frequency spectrum from a single bistable SR system are shown in Fig. 16b. However, the target signal was still indistinguishable in the time-domain waveform, and the low-frequency interference significantly worsened in the frequency spectrum, completely obscuring the target spectral signal. This indicates that a single SR system is ineffective in enhancing the target spectral signal under large parameter conditions. The outcome of CSR processing is presented in Fig. 16c, showing that the optimal cascade layer is 1, indicating that the effect of traditional CSR is inferior to that of a single SR system under large-parameter conditions in this experiment. The output result of CSR with the high-pass filter method is shown in Fig. 16d, with the optimal cascade layer being 3. Although the low-frequency interference signals have been significantly reduced due to the high-pass filter, the portion of the signal beyond the filter's designated cutoff frequency continues to manifest substantial interference, making it challenging to effectively extract the target line spectrum signal. Finally, the optimal output achieved by employing the proposed MIFF-CSR method is presented in Fig. 16e, where the signal waveform is perfectly restored, and the target spectral signal is clearly visible in the frequency spectrum. The output results in Fig. 16 demonstrate that the MIFF-CSR method effectively enhances target signals acquired in real-world scenarios. It exhibits a narrow band-pass filtering characteristic, effectively mitigating both high- and low-frequency interference. In contrast, the CSR method is ineffective, resulting in significant interference in both frequency regions. Similarly, the CSR with a high-pass filter method fails to eliminate interferences. Moreover, the MIFF-CSR method achieves a significantly higher output SNR, surpassing 25.59 dB compared to SR and CSR methods and exceeding CSR with a high-pass filter method by more than 20.79 dB, highlighting its substantial advantage in SNR enhancement for practical applications.

Figure 17 presents the average output SNR variation with cascaded layers. The MIFF-CSR method demonstrates robust tolerance toward the choice of cascaded layers in real-world scenarios, as increasing the cascaded layers does not adversely affect its performance. In practical applications, selecting cascaded layers for MIFF-CSR requires careful consideration of both signal characteristics and computational complexity. In cases with limited signal sampling rates that may impede SR, opting for a higher number of cascaded layers (around 15–30) within the acceptable computational capacity is advisable. The impact of the high-pass filter cutoff frequency in real-world scenarios is illustrated in Fig. 18. The output SNR remains relatively stable as the cutoff frequency varies, indicating that the MIFF-CSR method offers flexibility and high tolerance toward the high-pass filter cutoff frequency. Comparing the output SNR curves of MIFF-CSR, CSR, and CSR with a high-pass filter (as depicted in Fig. 17), we observe that the output SNR of MIFF-CSR continues to increase and stabilizes as the number of cascaded layers increases. In contrast, CSR and CSR with high-pass filter assistance show declining output SNR with limited cascaded layers, thus limiting their cascading effectiveness. This demonstrates that the proposed MIFF-CSR

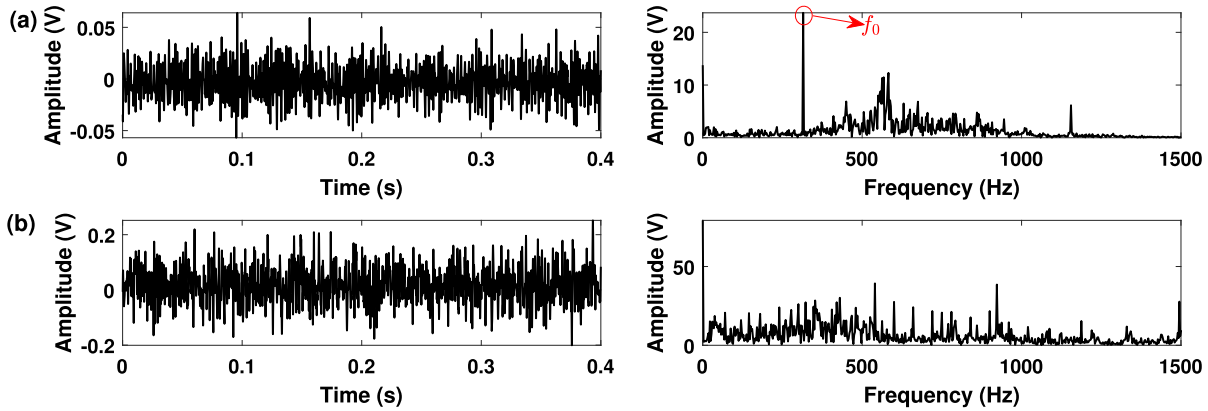

Fig. 15 Received noisy signal and background noise: **a** the time waveform and frequency spectrum of the original received noisy signal, **b** environment background noise amplified by a factor of 5

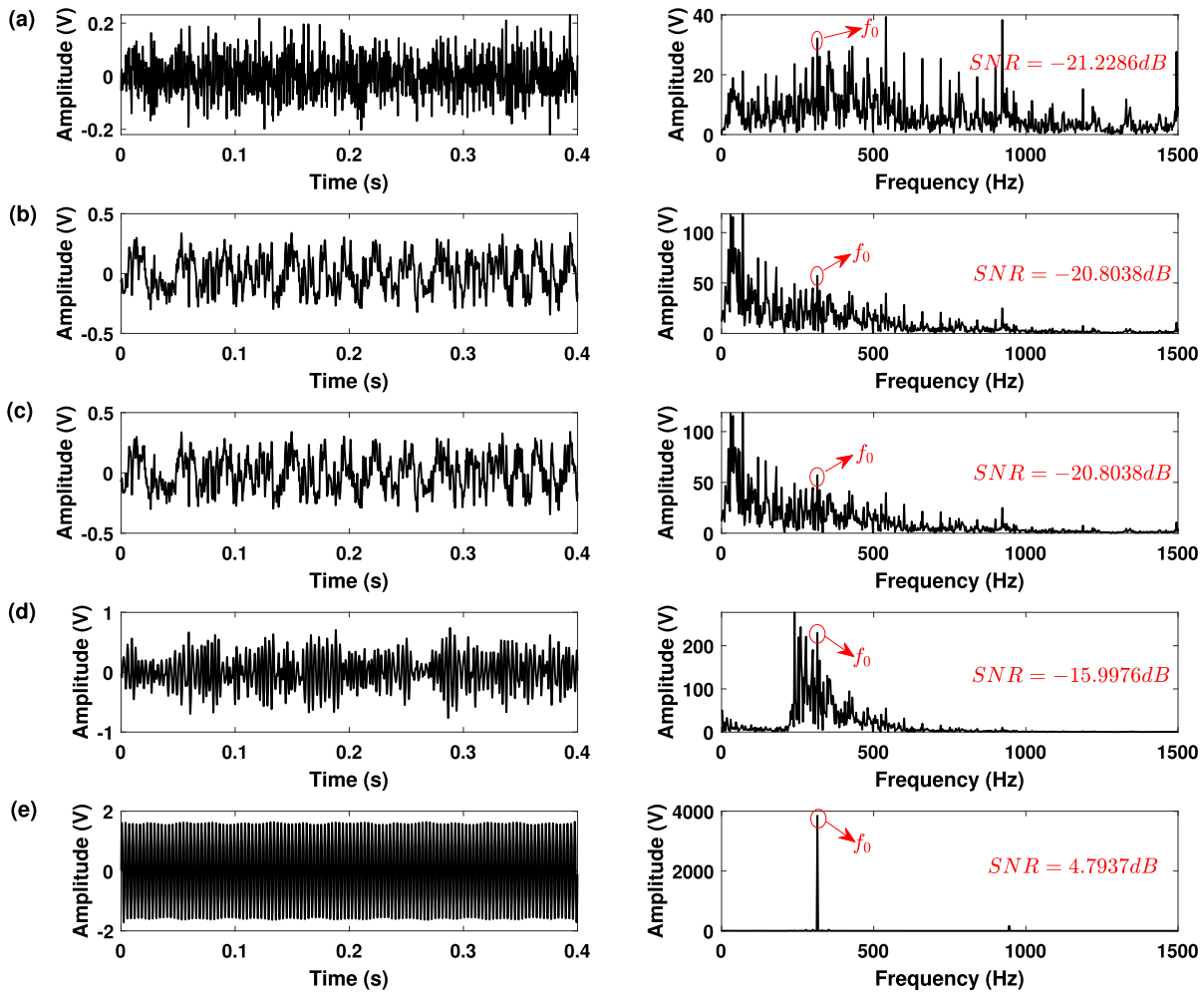

Fig. 16 Application verification: **a** the time waveform and frequency spectrum of the original received signal, **b** the output of single SR system, **c** the output of CSR, **d** the output of CSR with high-pass filter, **e** the output of proposed MIFF-CSR method

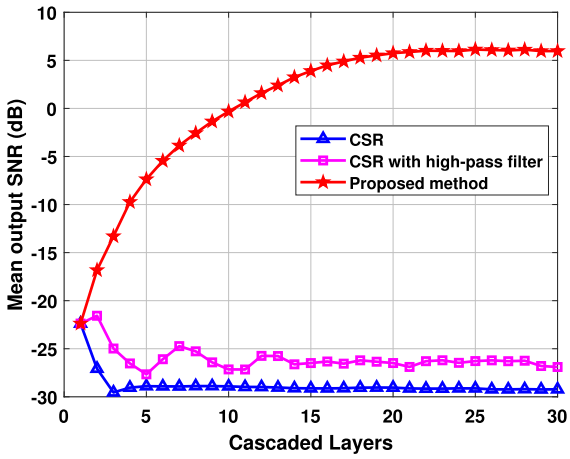

Fig. 17 The variations of mean output SNR with cascaded layers

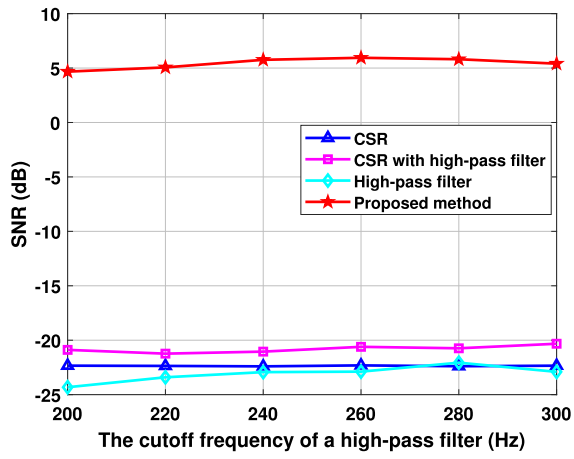

Fig. 18 The variations of mean output SNR with high-pass filter cutoff frequency

method yields superior signal processing performance and exhibits better adaptability in selecting the number of cascaded layers in practical applications. Furthermore, a comparison of the multiple curves in Fig. 17 and Fig. 18 reveals that the MIFF-CSR method significantly outperforms the other two methods, achieving an optimal average output SNR of over 25 dB. Moreover, in this experiment, the ratio of the signal frequency in the sampling frequency domain is 12 kHz/315 Hz = 38.09, which falls short of the required 50-fold for SR processing [14]. Under such conditions, SR, CSR, and CSR with high-pass filter methods exhibit unsatisfactory performance, as observed in Fig. 16. In contrast, the proposed MIFF-CSR method maintains excellent effectiveness, thereby affirming its suitability in real-world scenarios characterized by limited sampling rates. These analytical findings corroborate the practical viability and superior performance of the MIFF-CSR method in real-world applications.

5.2 Discussion

In this subsection, we present some discussions on the MIFF-CSR method,

(1) The proposed method is a fundamental framework, and in this study, we constructed the MIFF-CSR method based on the classical bistable SR model [43], known as the CBSR. Other SR models, such as the second-order SR system [44], the multistable SR system [45,46], and other special SR system [47], which exhibit better performance than CBSR, can also be applied to the proposed framework.

(2) Although the simulations in this study were conducted using Gaussian white noise, oceanic environmental noise that follows the α-stable distribution [48] or other pertinent models. In particular, SR can show more significant advantages in the presence of colored noise than white noise under certain circumstances [49]. Previous studies have also shown that SR performs well in processing colored noise [50] in the marine environment [51]. Although the background noise used in our experiment verification did not belong to Gaussian white noise, we still need to analyze the specific performance of MIFF-CSR under colored noise backgrounds.

(3) Given the intricate nature of nonlinear SR theory, particularly concerning traditional CSR with its limited theoretical underpinning, the theoretical derivation of MIFF-CSR presented in this study still needs to be improved. In the future, we will conduct further in-depth research to provide theoretical proof for MIFF-CSR.

(4) The outcomes of this research exemplify the significant advantages of cascaded-type SR, received signal feed-forward, and common information feed-forward. This approach can provide a strong basis for the future development of SR networks. We firmly believe that SR networks based on the proposed MIFF-CSR method will yield even more

remarkable results. This will be the primary focus of our next research direction.

6 Conclusion

This paper proposes a novel mutual information-assisted feed-forward cascaded stochastic resonance (MIFF-CSR) method, which employs mutual information and high-pass filtering to address the problem of severe low-frequency interference and dependence on each layer in large parameter cascade stochastic resonance (CSR) systems. The MIFF-CSR method incorporates a high-pass filter to attenuate low-frequency interference within large parameter SR. It employs cross-spectral analysis to extracts the mutual information between the high-pass filtered SR output signal and the original noisy signal. The extracted mutual information is subsequently forwarded to the next layer SR system, preventing interference from the previous layer SR to the subsequent layer. In order to prevent the poor response of any individual layer SR from adversely affecting the overall system, the original information is fed forward to each layer SR system. This decouples the strong dependence on each layer SR within CSR, leading to MIFF-CSR's enhanced stability and superior signal processing performance. The proposed MIFF-CSR method typically achieves a remarkable SNR improvement of exceeding 20 dB with a modest 5–6 layer configuration. Even under challenging conditions, such as limited sampling rates unfavorable for SR, the MIFF-CSR method still yields satisfactory results by employing more cascading layers. However, the excess cascading does not lead to performance degradation, as observed in CSR, highlighting the MIFF-CSR method's superior tolerance for selecting cascaded layers. Moreover, the study on the relationship between the cutoff frequency of the high-pass filter and the performance of the MIFF-CSR method confirms that there is a large selection space for the cutoff frequency, and the filtering performance has strong robustness within a certain range of cutoff frequencies. In addition, the simulation results further emphasize the superior performance of the proposed MIFF-CSR method compared to SR, CSR, and CSR with high-pass filter methods. It effectively mitigates severe low-frequency interference in large-parameter CSR and exhibits progressive enhancements in SNR and target signal restoration. Additionally, the MIFF-CSR method outperforms the other comparative methods, demonstrating a broader frequency response range, improved filtering performance with band-pass characteristics, and superior anti-noise capabilities. Application verification also confirms that the MIFF-CSR method has perfect environmental noise adaptability and can effectively restore waveform while exhibiting good band-pass filtering characteristics compared to SR, CSR, and high-pass filtering-assisted CSR methods. We expect that the proposed method can serve as a fundamental building block for future SR networks and provide a feasible path for improving the performance of complex SR systems.

Author contributions JS was involved in the conceptualization, methodology, software, validation, writing—original draft preparation. HW contributed to the data curation, project administration, and writing—review and editing. XS assisted in the supervision and writing—review and editing. YY contributed to the data curation and resources. HD performed the investigation and supervision.

Funding The authors declare that no funds, grants, or other support was received during the preparation of this manuscript. This work was supported by the National Natural Science Foundation of China (Grant No.62031021, 62271404, 62201439), China Postdoctoral Science Foundation (Grant No.2022M722493), and sponsored by Innovation Foundation for Doctor Dissertation of Northwestern Polytechnical University(Grant No.CX2022024). The authors would like to thank the anonymous reviewers for their valuable comments and suggestions.

Data availability The datasets generated during and/or analyzed during the current study are available from the corresponding author on reasonable request.

Declarations

Conflict of interest The authors have no relevant financial or non-financial interests to disclose.

References

1. Hänggi, P.: Stochastic resonance in biology how noise can enhance detection of weak signals and help improve biological information processing. ChemPhysChem **3**(3), 285–290 (2002)
2. Lu, S.L., Zheng, P., Liu, Y.B., Cao, Z., Yang, H., Wang, Q.J.: Sound-aided vibration weak signal enhancement for bearing fault detection by using adaptive stochastic resonance. J. Sound Vib. **449**, 18–29 (2019)
3. Rovňaková, J., Kocur, D.: Weak signal enhancement in radar signal processing. In: 20th International Conference Radioelektronika 2010, pp. 1–4 (2010)
4. Dong, H.T., Shen, X.H., He, K., Wang, H.Y.: Nonlinear filtering effects of intrawell matched stochastic resonance with

barrier constrainted duffing system for ship radiated line signature extraction. Chaos Solitons Fractals **141**, 110428 (2020)
5. Lu, S.L., He, Q.B., Wang, J.: A review of stochastic resonance in rotating machine fault detection. Mech. Syst. Signal Proc. **116**, 230–260 (2019)
6. Gammaitoni, L., Hänggi, P., Jung, P., Marchesoni, F.: Stochastic resonance: a remarkable idea that changed our perception of noise. Eur. Phys. J. B **69**, 1–3 (2009)
7. Qiao, Z.J., Lei, Y.G., Li, N.P.: Applications of stochastic resonance to machinery fault detection: a review and tutorial. Mech. Syst. Signal Process. **122**, 502–536 (2019)
8. Leng, Y.G., Wang, T.Y., Guo, Y., Xu, Y.G., Fan, S.B.: Engineering signal processing based on bistable stochastic resonance. Mech. Syst. Signal Process. **21**(1), 138–150 (2007)
9. Benzi, R., Sutera, A., Vulpiani, A.: The mechanism of stochastic resonance. J. Phys. A Math. Gen. **14**(11), 453 (1981)
10. Moss, F., Ward, L.M., Sannita, W.G.: Stochastic resonance and sensory information processing: a tutorial and review of application. Clin. Neurophysiol. **115**(2), 267–281 (2004)
11. Shen, M.G., Yang, J.H., Jiang, W.B., Sanjuan, M.A., Zheng, Y.Q.: Stochastic resonance in image denoising as an alternative to traditional methods and deep learning. Nonlinear Dyn. **109**(3), 2163–2183 (2022)
12. Brooker, A., Humphrey, V.: Measurement of radiated underwater noise from a small research vessel in shallow water. Ocean Eng. **120**, 182–189 (2016)
13. Xu, B.H., Duan, F.B., Bao, R.H., Li, J.L.: Stochastic resonance with tuning system parameters: the application of bistable systems in signal processing. Chaos Solitons Fractals **13**(4), 633–644 (2002)
14. Leng, Y.G., Leng, Y.S., Wang, T.Y., Guo, Y.: Numerical analysis and engineering application of large parameter stochastic resonance. J. Sound Vib. **292**(3–5), 788–801 (2006)
15. Li, Q., Wang, T.Y., Leng, Y.G., Wang, W., Wang, G.F.: Engineering signal processing based on adaptive step-changed stochastic resonance. Mech. Syst. Signal Process. **21**(5), 2267–2279 (2007)
16. Tan, J.Y., Chen, X.F., Wang, J.Y., Chen, H.X., Cao, H.R., Zi, Y.Y., He, Z.J.: Study of frequency-shifted and re-scaling stochastic resonance and its application to fault diagnosis. Mech. Syst. Signal Process. **23**(3), 811–822 (2009)
17. Li, J.M., Wang, X.D., Li, Z.X., Zhang, Y.G.: Stochastic resonance in cascaded monostable systems with double feedback and its application in rolling bearing fault feature extraction. Nonlinear Dyn. **104**, 971–988 (2021)
18. He, H.L., Wang, T.Y., Leng, Y.G., Zhang, Y., Li, Q.: Study on non-linear filter characteristic and engineering application of cascaded bistable stochastic resonance system. Mech. Syst. Signal Process. **21**(7), 2740–2749 (2007)
19. Li, J.M., Zhang, Y.G., Xie, P.: A new adaptive cascaded stochastic resonance method for impact features extraction in gear fault diagnosis. Measurement **91**, 499–508 (2016)
20. Neiman, A., Schimansky-Geier, L.: Stochastic resonance in two coupled bistable systems. Phys. Lett. A **197**(5–6), 379–386 (1995)
21. Li, J.M., Zhang, J.F., Li, M., Zhang, Y.G.: A novel adaptive stochastic resonance method based on coupled bistable systems and its application in rolling bearing fault diagnosis. Mech. Syst. Signal Process. **114**, 128–145 (2019)
22. Zhang, G., Zeng, Y.J., Zhang, T.Q.: Second-order coupled tristable stochastic resonance and its application in bearing fault detection under different noises. Nonlinear Dyn. **111**(10), 8987–9009 (2023)
23. Yan, Z., Guirao, J.L., Saeed, T., Chen, H.T., Liu, X.B.: Analysis of stochastic resonance in coupled oscillator with fractional damping disturbed by polynomial dichotomous noise. Nonlinear Dyn. **110**(2), 1233–1251 (2022)
24. Tessone, C.J., Toral, R.: System size stochastic resonance in a model for opinion formation. Phys. A **351**(1), 106–116 (2005)
25. Wang, Q.B., Wu, H., Yang, Y.J.: The effect of fractional damping and time-delayed feedback on the stochastic resonance of asymmetric SD oscillator. Nonlinear Dyn. **107**, 2099–2114 (2022)
26. Ma, T.C., Song, D., Shen, J.X., Xu, F.Y.: Unsaturated piecewise bistable stochastic resonance with three kinds of asymmetries and time-delayed feedback. Chaos Solitons Fractals **161**, 112352 (2022)
27. Kim, J., Harne, R.L., Wang, K.-W.: Online signal denoising using adaptive stochastic resonance in parallel array and its application to acoustic emission signals. J. Vib. Acoust. **144**(3), 031006 (2022)
28. Zhang, X.F., Hu, N.Q., Hu, L., Cheng, Z.: Multi-scale bistable stochastic resonance array: A novel weak signal detection method and application in machine fault diagnosis. Sci. China Inf. Sci. **56**, 2115–2123 (2013)
29. Tuo, X.H., Yang, X.L.: How synaptic plasticity affects the stochastic resonance in a modular neuronal network. Nonlinear Dyn. **110**(1), 791–802 (2022)
30. Yang, X.L., Li, N., Sun, Z.K.: Extended analysis of stochastic resonance in a modular neuronal network at different scales. Nonlinear Dyn. **98**, 1029–1039 (2019)
31. Suo, J., Wang, H.Y., Lian, W., Dong, H.T., Shen, X.H., Yan, Y.S.: Feed-forward cascaded stochastic resonance and its application in ship radiated line signature extraction. Chaos Solitons Fractals **174**, 113812 (2023)
32. Singh, M., Verma, A., Sharma, N.: An optimized cascaded stochastic resonance for the enhancement of brain MRI. Irbm **39**(5), 334–342 (2018)
33. Xiao, L., Bajric, R., Zhao, J.S., Tang, J.X., Zhang, X.H.: An adaptive vibrational resonance method based on cascaded varying stable-state nonlinear systems and its application in rotating machine fault detection. Nonlinear Dyn. **103**, 715–739 (2021)
34. Zhao, R., Yan, R.Q., Gao, R.X.: Dual-scale cascaded adaptive stochastic resonance for rotary machine health monitoring. J. Manuf. Syst. **32**(4), 529–535 (2013)
35. Li, J.M., Cheng, X., Peng, J.L., Meng, Z.: A new adaptive parallel resonance system based on cascaded feedback model of vibrational resonance and stochastic resonance and its application in fault detection of rolling bearings. Chaos Solitons Fractals **164**, 112702 (2022)
36. Gong, T., Yang, J.H., Liu, S.Y., Liu, H.G.: Non-stationary feature extraction by the stochastic response of coupled oscillators and its application in bearing fault diagnosis under variable speed condition. Nonlinear Dyn. **108**(4), 3839–3857 (2022)
37. Yu, Y., She, K., Liu, J.H., Cai, X., Shi, K.B., Kwon, O.: A super-resolution network for medical imaging via transfor-

mation analysis of wavelet multi-resolution. Neural Netw. **166**, 162–173 (2023)
38. Lai, W.S., Huang, J.B., Ahuja, N., Yang, M.-H.: Fast and accurate image super-resolution with deep laplacian pyramid networks. IEEE Trans. Pattern Anal. Mach. **41**(11), 2599–2613 (2018)
39. Gammaitoni, L., Hänggi, P., Jung, P., Marchesoni, F.: Stochastic resonance. Rev. Mod. Phys. **70**(1), 223 (1998)
40. Lu, S.L., He, Q.B., Zhang, H.B., Kong, F.R.: Enhanced rotating machine fault diagnosis based on time-delayed feedback stochastic resonance. J. Vib. Acoust. **137**(5), 051008 (2015)
41. He, Q.B., Wang, J., Liu, Y.B., Dai, D.Y., Kong, F.R.: Multiscale noise tuning of stochastic resonance for enhanced fault diagnosis in rotating machines. Mech. Syst. Signal Process. **28**, 443–457 (2012)
42. Johnson, J.M., Rahmat-Samii, V.: Genetic algorithms in engineering electromagnetics. IEEE Antennas Propag. Mag. **39**(4), 7–21 (1997)
43. Fauve, S., Heslot, F.: Stochastic resonance in a bistable system. Phys. Lett. A **97**(1–2), 5–7 (1983)
44. Qiao, Z.J., Elhattab, A., Shu, X.D., He, C.B.: A second-order stochastic resonance method enhanced by fractional-order derivative for mechanical fault detection. Nonlinear Dyn. **106**, 707–723 (2021)
45. Li, J.M., Chen, X.F., He, Z.J.: Multi-stable stochastic resonance and its application research on mechanical fault diagnosis. J. Sound Vib. **332**(22), 5999–6015 (2013)
46. Lai, Z., Liu, J., Zhang, H., Zhang, C., Zhang, J., Duan, D.: Multi-parameter-adjusting stochastic resonance in a standard tri-stable system and its application in incipient fault diagnosis. Nonlinear Dyn. **96**, 2069–2085 (2019)
47. Qiao, Z.J., Chen, S., Lai, Z.H., Zhou, S.T., Sanjuán, M.A.: Harmonic-gaussian double-well potential stochastic resonance with its application to enhance weak fault characteristics of machinery. Nonlinear Dyn. **111**(8), 7293–7307 (2023)
48. Wang, C.C., Liao, M.S., Li, X.F.: Ship detection in SAR image based on the alpha-stable distribution. Sensors **8**(8), 4948–4960 (2008)
49. Nozaki, D., Mar, D.J., Grigg, P., Collins, J.J.: Effects of colored noise on stochastic resonance in sensory neurons. Phys. Rev. Lett. **82**(11), 2402 (1999)
50. Yamakou, M.E., Tran, T.D.: Lévy noise-induced self-induced stochastic resonance in a memristive neuron. Nonlinear Dyn. **107**(3), 2847–2865 (2022)
51. Ji, S.Y., Yuan, F., Yu, C.K., Cheng, E.: Application of stochastic resonance technology in underwater acoustic weak signal detection. In: OCEANS 2016-Shanghai, pp. 1–5 (2016)